Available online at www.sciencedirect.com
SCIENCE DIRECT®
Journal of Solid State Chemistry 178 (2005) 1080–1086
JOURNAL OF SOLID STATE CHEMISTRY
www.elsevier.com/locate/jssc

Synthesis and characterization of $Zn_{1-x}Ni_xFe_2O_4$ spinels prepared by a citrate precursor

Mona Mouallem-Bahout*, Sarah Bertrand, Octavio Peña

Laboratoire de Chimie du Solide et Inorganique Moléculaire, UMR 6511 CNRS, Université de Rennes 1, Institut de Chimie de Rennes, 35042 Rennes, Cedex, France

Received 1 September 2004; received in revised form 2 December 2004; accepted 13 January 2005

Abstract

Nanocrystalline single-phase samples of $Zn_{1-x}Ni_xFe_2O_4$ ferrites ($0<x<1$) have been obtained via a soft-chemistry method based on citrate–ethylene glycol precursors, at a relatively low temperature (650 °C). The influence of the nickel and zinc contents as well as that of heat treatments were investigated by means of X-ray powder diffraction, Brunauer–Emmett–Teller (BET) surface area, scanning electron microscopy (SEM) and Fourier Transform Infrared (FTIR) Spectroscopy. Higher Ni content increases the surface areas, the largest one (~20 m^2/g) being obtained for $NiFe_2O_4$ annealed at 650 °C for 15 h. For all compositions, the surface area decreases for prolonged annealing at 650 °C and for higher annealing temperatures. Those results were correlated to the particle size evolution; the smallest particles (~50 nm) observed in the $NiFe_2O_4$ sample (650 °C, 15 h) steadily increase as Ni ions were replaced by Zn, reaching ~100 nm in the $ZnFe_2O_4$ sample (650 °C, 15 h). For all the $Zn_{1-x}Ni_xFe_2O_4$ samples and, whatever the heat treatments was, the FTIR spectra show two fundamental absorption bands in the range 650–400 cm^{-1}, characteristics of metal vibrations, without any superstructure stating for cation ordering. The highest v_1-tetrahedral stretching, observed at ~615 cm^{-1} in $NiFe_2O_4$, shifts towards lower values with increasing Zn, whereas the v_2-octahedral vibration, observed at 408 cm^{-1} in $NiFe_2O_4$, moves towards higher wavenumbers, reaching 453 cm^{-1} in $ZnFe_2O_4$.

Keywords: Nanocrystalline ferrites; Powder X-ray diffraction; Specific surface area; SEM; FTIR

1. Introduction

AFe_2O_4 ferrospinels are attractive as electronic devices as they cover a range of applications from low wavenumber to microwave and from low to high permeability. The unit cell contains 32 O-atoms in a cubic closest packing with eight tetrahedral and 16 octahedral occupied sites. In the "normal" structure, the divalent A-cations enter fourfold tetrahedral coordination, and ferric ions occupy the octahedral sites. In the "inverse" structure, much common in ferrites, the A-cations move to the octahedral sites and are replaced by half the Fe ions in the tetrahedral sites, the second half of Fe ions remaining at the octahedral sites. Intermediate configurations, generally temperature-dependent, often occur; and the inversion parameter, γ accounts for the ratio of the divalent A-ions at the octahedral site.

The crystalline and magnetic properties of polycrystalline (Ni, Zn) ferrites have been intensively studied since 50s because of their high permeability in the radio frequency region. The magnetic characteristics are sensitive to composition, as well as to the synthesis route and grain size. Moreover, polycristalline ferrites are considered as important catalysts for CO_2 and H_2O decomposition [1] and attractive gas sensors for reducing gases like liquefied petroleum gas, ethanol, CO and CH_4 [2].

*Corresponding author. Fax: +33 2 23 23 67 99.
E-mail address: mona.bahout@univ-rennes1.fr (M. Mouallem-Bahout).

0022-4596/$ - see front matter © 2005 Elsevier Inc. All rights reserved.
doi:10.1016/j.jssc.2005.01.009

The large work on (Ni, Zn) ferrites has been carried out on microcrystalline ceramics prepared by the standard ceramic technique, involving high-temperature reactions between finely milled oxide (or carbonate) powders followed by shaping and successive pressing and sintering [3,4]. Because the magnetic properties and gas sensitivity of (Ni, Zn)-ferrites largely depend on composition and grain size of the polycrystalline samples, it is necessary to examine the effect of heat treatments on the microstructure of some selected compositions of the (Ni, Zn)Fe_2O_4 system in order to tune ferrite samples with the required characteristics. The present work is focused on the properties of a series of nanocrystalline ferrites, $Zn_{1-x}Ni_xFe_2O_4$; ($x = 0$, 0.25, 0.50, 0.75, 1), obtained via a soft-chemistry route, from citrate precursors. The X-ray powder diffraction patterns, the Brunauer–Emmett–Teller surface areas (BET), the microstructure and the infrared (IR) properties are discussed as a function of composition and heat treatments.

2. Experimental

2.1. Synthesis

Nanocrystalline $Zn_{1-x}Ni_xFe_2O_4$ ferrites were prepared via the Pechini process, from citrate–ethylene glycol precursors [5], by dissolving stoichiometric amounts of $Ni(NO_3)_2 \cdot 6H_2O$, $Zn(NO_3)_2 \cdot 6H_2O$ and $Fe(NO_3)_3 \cdot 9H_2O$ (Acros, purity > 98%) in distilled water and adding them to an aqueous warm solution (40 °C) of citric acid/ethylene glycol (~0.25 mol of citric acid and ~1 mol of ethylene glycol were used for obtaining ~5 g of a ferrite sample) under continuous stirring. A small amount of nitric acid was added to adjust the pH of the solution to pH < 2 that was heated at 80 °C for 2 h to achieve complete chelation. The temperature was then raised to ~150 °C for water evaporation and chelates polyesterification. A yellow viscous gel was obtained rapidly transforming into a dark-brown amorphous resin which was first dried on a heat plate at ~220 °C, then furnace-heated at 550 °C for 24 h, under air, for organic material combustion. The resulting powder was ground, spread in an alumina crucible and calcinated, under air, at 650 °C for 15 h (or 700 °C for 6 h) then, separated in three batches and heated at 800 °C (15 h), 900 °C (15 h) or 1200 °C (4 h). The furnace was then shut off for samples to reach room temperature. In order to investigate the shaping effect upon the crystal growth, the 700 °C heated $Zn_{0.5}Ni_{0.5}Fe_2O_4$ powder was pressed into pellet and sintered at 800 °C (6 h).

2.2. Crystal structure

Powder X-ray diffraction (XRD) analyses were performed using a calibrated CPS 120 INEL X-ray powder diffractometer equipped with a position-sensitive detector operating at 40 kV/25 mA with a flat geometry, using Cu$K\alpha$ radiation. The structure refinement was carried out with the Fullprof software [6,7]. A pseudo-Voigt function was used to describe the instrumental and sample contribution to the peak profile and the FWHM was parameterized as $\sigma^2 = utg^2\theta + vtg\theta + w$. The background was modeled by means of a linear interpolation of ~25 points. The cell parameter, the oxygen coordinates, the isotropic displacement parameters and the instrumental parameters u, v, w were allowed to vary during the structure refinement.

2.3. Scanning electron microscope-energy dispersive spectrometry (SEM-EDS)

Semiquantitative microprobe analyses were performed with a JEOL JSM-6400 Scanning Electron Microscope (SEM) equipped with an Oxford Energy Dispersive Spectroscopy (EDS) detector. Small amounts of powder were spread on a scotch tape, sputtered with a very thin film of carbon. Data were acquired with an accelerating voltage of 20 kV and accumulation time of 45 s. The EDS analyses were in good agreement with the expected ratios of the transition metals Fe, Ni and Zn proving that the citrate–ethylene glycol method was able to yield ceramics of high elemental uniformity.

SEMs were obtained using a JEOL-JSM-6301 operating at 9 kV.

2.4. Brunauer–Emmett–Teller (BET)

The specific surface area of the oxide powders was determined by the single-point BET calculation method using N_2 gas.

2.5. Fourier transform infrared spectroscopy (FTIR)

Infrared (IR) spectra of dried ferrite samples were recorded on the Brüker Equinox FTIR spectrophotometer in the range of 4000–400 cm^{-1}. Sample preparation included mixing ferrite powder with KBr powder (~10 mg ferrite/~300 mg KBr). Because KBr is highly hygroscopic, it was dried before using and the pellets were prepared under inert atmosphere.

3. Results and discussion

3.1. Crystal structure refinement

The XRD patterns of all the $Zn_{1-x}Ni_xFe_2O_4$ samples show the characteristic reflections of the *Fd*3*m* cubic spinel group. Typical diagrams of $ZnFe_2O_4$ samples, heated at 650 and 800 °C, shown in Fig. 1, indicate that the citrate–ethyleneglycol precursor method led to ferrite-spinels at a low synthesis temperature. However,

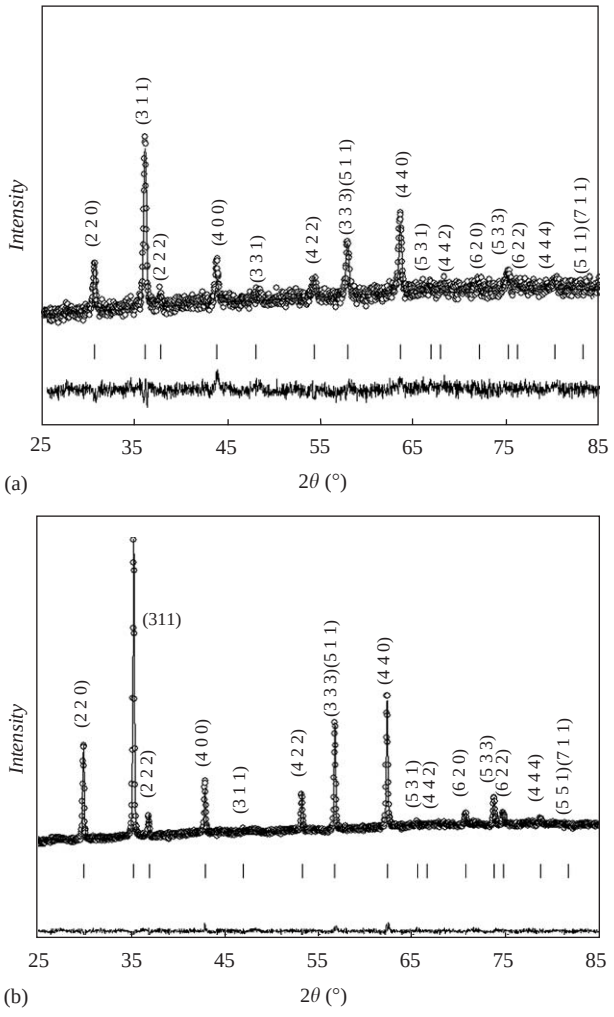

Fig. 1. Powder XRD patterns of $ZnFe_2O_4$ heated at 650 °C (a) and 800 °C (b). The circles are the experimental data and the solid lines are the calculated profiles in the *Fd3m* space group. The lower traces show the differences between the experimental and calculated data. The tick marks denote the positions of the expected reflections.

the 650 °C pattern is characterized by a low crystallinity reflected by high reliability factors, $R_B = 28.4\%$ and $R_f = 26.2\%$, whereas the X-ray diagram of the 800 °C annealed sample shows a clear sharpness of the X-ray lines and led to a reasonable agreement between the theoretical and calculated diagrams, with $R_B = 3.26\%$ and $R_f = 4.06\%$. Heating at 900 and 1200 °C improves the crystallinity of the $Zn_{1-x}Ni_xFe_2O_4$ samples but led to no significant changes of the lattice parameters which were in good agreement with the values reported for solid solutions prepared by the solid state reaction [8].

Fig. 2 shows that the diffraction patterns of the $Zn_{1-x}Ni_xFe_2O_4$ samples ($x = 0$, 0.25, 0.5, 0.75, 1) shift towards higher 2θ values when x increases. The decreasing of the lattice parameter from 8.439 to 8.359 Å as x varies from 0 to 1 (Table 1) is attributed to the smaller ionic radius of Ni^{2+} (0.69 Å) in comparison to that of Zn^{2+} (0.74 Å).

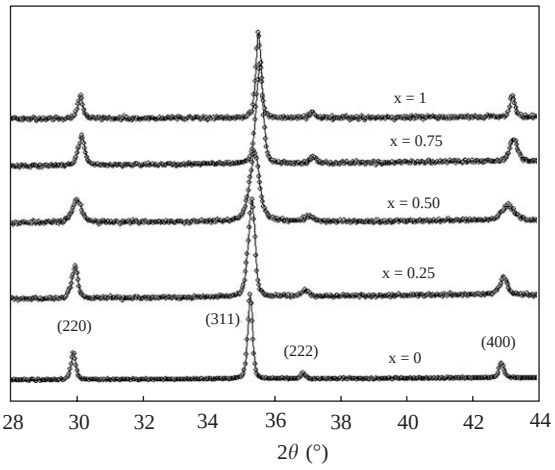

Fig. 2. XRD patterns of $Zn_{1-x}Ni_xFe_2O_4$ annealed at 800 °C ($\lambda = 1.54056$ Å) as a function of Ni content (x). The peaks are indexed in the *Fd3m* cubic space group.

Table 1
Lattice parameters of the $Zn_{1-x}Ni_xFe_2O_4$ compounds, refined from the X-ray diffraction patterns of the samples annealed at 800 °C (15 h)

x	a (Å)
0	8.439
0.25	8.421
0.5	8.402
0.75	8.368
1	8.359

Usually, $ZnFe_2O_4$ is a normal spinel, with Zn ions at the tetrahedral sites and Fe^{3+} ions at the octahedral site, whereas, $NiFe_2O_4$ and $Ni_xFe_{3-x}O_4$ are inverse spinels the high stabilization of Ni ions in octahedral coordination is associated with the migration of a corresponding amount of Fe^{3+} ions to tetrahedral positions [9]. However, O'-Neill et al. reported that in high-temperature annealed $ZnFe_2O_4$ samples, quenched to room temperature, a partial site exchange occurs between tetrahedral Zn^{2+} and octahedral Fe^{3+} ions [10]. Moreover, Shinoda and his coworkers stated that upon milling nanocrystalline $NiFe_2O_4$ bulk material, some Ni^{2+} ions move to tetrahedral sites [11].

Usually, cation distribution is temperature-dependent in most of the spinel oxides [12–15] and O'Neill and Navrotsky described the inversion parameter of ion exchange between tetrahedral and octahedral sites by means of a conventional thermodynamic model [16]. In order to check the temperature dependence of the cation distribution, various ferrite samples, $Zn_{1-x}Ni_xFe_2O_4$ were annealed at 800, 900 or 1200 °C followed by furnace cooling. The XRD patterns showed a real improvement of the crystallinity but without any evidence for a site exchange or signs of cation ordering. Indeed, no additional superstructure reflections, nor

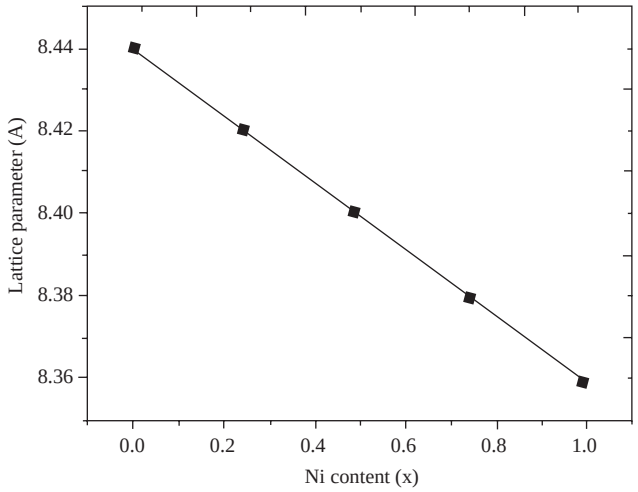

Fig. 3. Variation of the lattice parameter of the $Zn_{1-x}Ni_xFe_2O_4$ ferrites, refined from the powder X-ray patterns of the samples annealed at 800 °C (15 h).

significant changes in the diffraction lines intensity, even in the (220) one that exclusively depends on the tetrahedral cations, could be detected. Because of the poor chemical contrast between the X-ray scattering factors of the Fe, Zn and Ni, refinement of the fractional occupancies at the tetrahedral and octahedral sites was limited. This situation contrasts to that of the $Li_{0.5}Fe_{2.5}O_4/LiMn_2O_4$-system where substitution of Fe by Li ions led to additional superstructure reflection lines in the X-ray diagram consecutive to a lowering of the symmetry due to an ordering between the Li and Fe ions, easily detectable, because of a strong difference of the X-ray scattering factors [17,18].

Fig. 3 shows the evolution of the lattice parameter of the cubic cell throughout the (Zn, Ni)Fe_2O_4 system. The monotonous linear variation suggests that Ni and Fe ions are more likely disordered at the octahedral site of the $Zn_{1-x}Ni_xFe_2O_4$ spinels, in agreement with the results on most of the Zn-based ferrite spinels, $Zn_{1-x}M_xFe_2O_4$; M = Ni, Cu, Co, Mg [19,20]. This situation contrasts with that observed in the spinel-manganates, (Li,Fe)Mn_2O_4 [21] and $LiMn_{1.5}M_{0.5}O_4$, M = Mg, Ti, Co, Ni, Cu, Zn and Ga [22] where deviation from the linearity predicted by Vegard's law has been assigned to a crystal symmetry lowering from consecutive to a crystalline order between Li and Mn ions.

3.2. N_2 adsorption and SEM

N_2 adsorption/desorption isotherms of the ferrites heated at 650 °C ~15 h showed a clear mesoporous character. The specific surface areas of some selected compositions, $ZnFe_2O_4$, $Zn_{0.5}Ni_{0.5}Fe_2O_4$ and $NiFe_2O_4$, were ~12.06, 15.84 and 19.15 m^2/g, respectively. A prolonged heating (30 h) at 650 °C, investigated for the $ZnFe_2O_4$ compound, showed a clear decrease of the surface areas to ~6 m^2/g. A similar behavior occurs when the annealing temperature is raised to 800 °C (15 h), the surface area reaching 4.6 m^2/g. Investigations of heat treatment effects on the surface areas for the other compositions of the (Zn, Ni)Fe_2O_4 system are in progress.

The microstructure of the $Zn_{1-x}Ni_xFe_2O_4$ solid solutions was examined as a function of the heat treatments and composition. The SEMs of three selected compositions, $ZnFe_2O_4$, $Zn_{0.5}Ni_{0.5}Fe_2O_4$ and $NiFe_2O_4$ are shown in Fig. 4 for different annealing temperatures.

3.2.1. $ZnFe_2O_4$

The electron micrograph of the 650 °C heated compound (Fig. 4a) consists in agglomerated grains with visible grain boundaries. The grain-size distribution consists of a majority of well-defined spherical particles, ranging from 20 to 100 nm, with a maximum around 100 nm. When increasing the annealing temperature to 800 and 900 °C, the particles fused together and most of the grains grow to ~150 and 300 nm, respectively (Figs. 4b and 4c). For a sintered pellet at 1200 °C, 4 h, the material becomes highly dense and large particles of ~1 μm are observed (Fig. 4d). The maximum of the grain-size distribution of the $ZnFe_2O_4$ samples, as a function of the heating temperature, is listed in Table 2.

3.2.2. $Zn_{0.5}Ni_{0.5}Fe_2O_4$

The grain-size distribution of the 700 °C heated sample is very heterogeneous (Fig. 4e) and ranges from ~ 20 to ~ 90 nm.

When the powder is compacted into pellet and sintered at 800 °C (6 h), the grain-size distribution becomes more homogeneous (Fig. 4f), with a considerable crystallite growth; some of the crystallites reaching ~200 nm. Large domains of high density are observed in comparison to the much less porous 700 °C $Zn_{0.5}Ni_{0.5}Fe_2O_4$ specimen. Compacting the powder should considerably promote the crystallite growth.

3.2.3. $NiFe_2O_4$

The SEM micrograph of the 650 °C heated $NiFe_2O_4$ sample (Fig. 4(g)) show a relatively homogeneous grain distribution, consisting of well-crystallized grains, with an average grain size of about 50 nm, smaller than in the other compositions. The agglomerated particles form, either diluted aggregates or thick blocks and the grain boundaries are less marked in comparison to the 650 °C $ZnFe_2O_4$ sample. Upon increasing the annealing temperature to 800 °C (15 h), the grain size distribution become very heterogeneous (Fig. 4(h)).

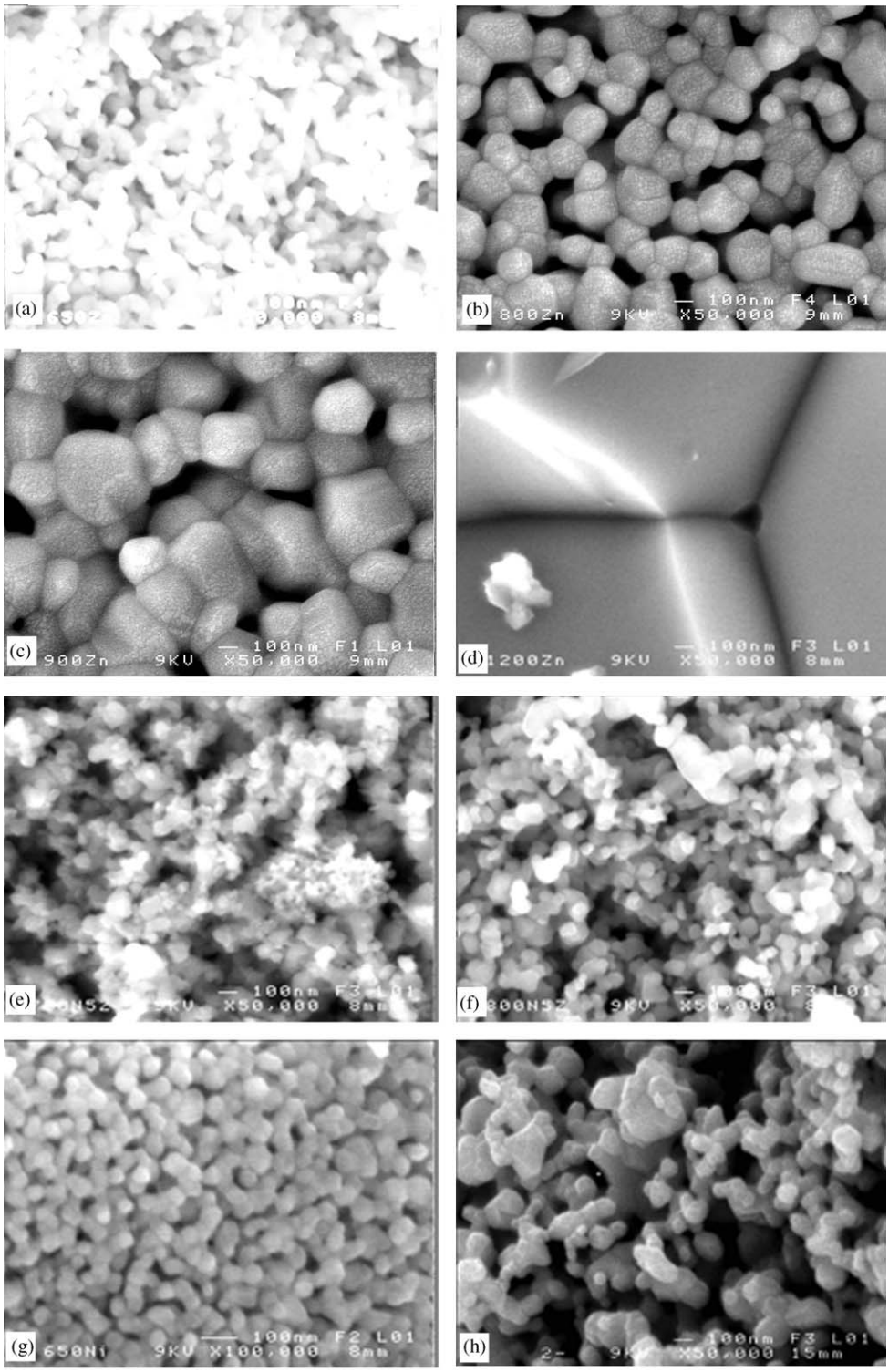

Fig. 4. SEM of $Zn_{1-x}Ni_xFe_2O_4$ samples annealed at various temperatures, $ZnFe_2O_4$: (a) 650 °C—15 h, (b) 800 °C—15 h, (c) 900 °C—15 h, (d) 1200 °C—4 h, $Zn_{0.5}Ni_{0.5}Fe_2O_4$: (e) 700 °C—6 h, (f) 800 °C—6 h, $NiFe_2O_4$: (g) 650 °C—15 h, (h) 800 °C—15 h. The powders were spread in alumina crucibles and heated, except for $Zn_{0.5}Ni_{0.5}Fe_2O_4$—800 °C that was pressed into pellet and sintered at 800 °C.

3.3. Infrared analysis

The IR spectra of the $Zn_{1-x}Ni_xFe_2O_4$ samples show small differences in the range 4000–1000 cm^{-1}. A typical spectrum of the $Zn_{0.5}Ni_{0.5}Fe_2O_4$ specimen, heated at 650 °C, 6 h is shown in Fig. 5.

This spectrum shows evidence for CO_3^{2-} and NO_3^- vibrations as well as for the presence of moisture. The

Table 2
Maximum of the grain size-distribution of $ZnFe_2O_4$ samples annealed at various temperatures for 15 h

Annealing temperature (°C)	Grain size (nm)
650	100
800	150
900	300
1200	1000

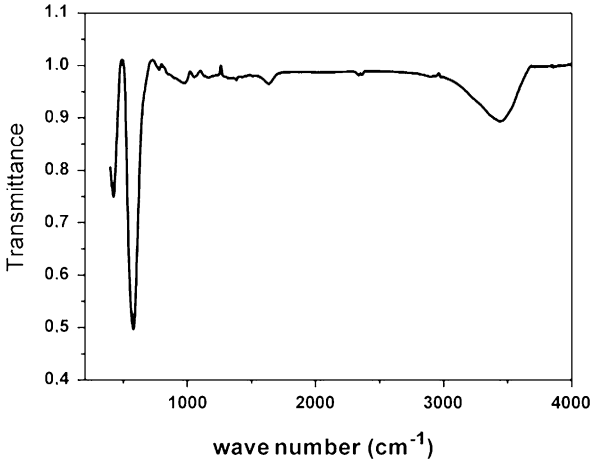

Fig. 5. IR spectrum of $Zn_{0.5}Ni_{0.5}Fe_2O_4$ annealed at 650 °C (6 h).

intensive broadband, around 3450 cm^{-1} is due to O↔H stretching vibration interacting through H bonds. The second one, observed at ~1600 cm^{-1}, is less intensive and the maximum of the third H_2O absorption band at ~900–1000 cm^{-1} indicates strong hydrogen bridges. Traces of adsorbed or atmospheric CO_2 are evidenced by the very light band around 2350 cm^{-1}. The ν(C=O) stretching vibration of the carboxylate group (CO_2^-) is observed around 1400 cm^{-1} and the band at ~1050 cm^{-1} would state for nitrate ions traces. As a consequence of a prolonged annealing at 650 °C (15 h), the CO_3^{2-} and CO_2^- vibrations disappear.

In the range 1000–100 cm^{-1}, the IR bands of solids are usually assigned to vibration of ions in the crystal lattice [23]. Two main broad metal–oxygen bands are seen in the IR spectra of all spinels, and ferrites in particular. The highest one, v_1, generally observed in the range 600–550 cm^{-1}, corresponds to intrinsic stretching vibrations of the metal at the tetrahedral site, M_{tetra}↔O, whereas the v_2-lowest band, usually observed in the range 450–385 cm^{-1}, is assigned to octahedral-metal stretching, M_{octa}↔O [24,25].

In the $Zn_{1-x}Ni_xFe_2O_4$ solid solutions, Ni^{2+} is stabilized in the octahedral crystal field whereas Zn^{2+} prefers tetrahedral sites because of its facility to form covalent bonds involving sp^3 hybrid orbitals. Consequently, the v_1 band, observed at ~561 cm^{-1} for

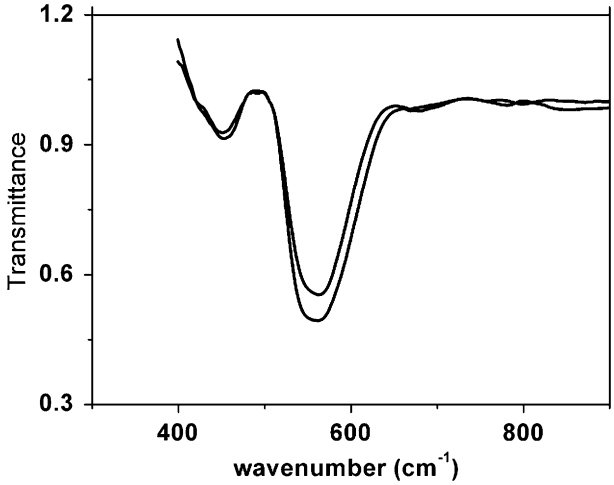

Fig. 6. IR spectrum of $ZnFe_2O_4$ annealed 15 h at 650 °C (lower) and 900 °C (upper).

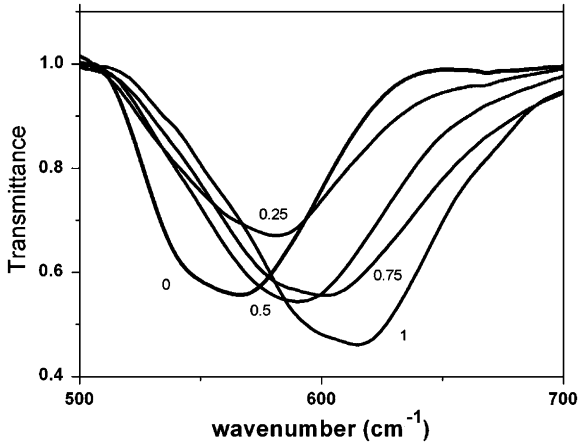

Fig. 7. IR spectra of $Zn_{1-x}Ni_xFe_2O_4$ (heated at 800 °C, 15 h) as a function of the Ni content (x).

$ZnFe_2O_4$ (Fig. 6) can be assigned to tetrahedral Zn^{2+} stretching and the v_2 band, observed at ~453 cm^{-1}, involves the Fe^{3+} vibration at the octahedral site. When increasing the annealing temperature to 900 °C, only a light variation of the relative intensity of the v_1 and v_2 bands is visible but no shift or fine structure are detectable (Fig. 6).

In the $Zn_{1-x}Ni_xFe_2O_4$ solid solutions, when tetrahedral Zn^{2+} are replaced by smaller Fe^{3+} ions with lower atomic weight, the v_1 vibration shifts to higher wavenumber, as shown in Fig. 7 and Table 3. On the other hand, the v_2-octahedral band displacement is so light that it is only noticed when comparing the end members, $ZnFe_2O_4$ and $NiFe_2O_4$.

Based on the factor group approximation, theory group predicts that the cubic *Fd3m* spinels, both inverse and normal, should display four IR active vibrations. However, if a cation ordering at the octahedral site exists, the number of active band should significantly

Table 3
FTIR vibrations for $Zn_{1-x}Ni_xFe_2O_4$ compounds sintered 15 h at 800 °C; v_1 and v_2 correspond to the transition ions stretching vibrations in tetrahedral an octahedral sites, respectively

Compound	v_1 (cm^{-1})	v_2 (cm^{-1})
$ZnFe_2O_4$	561	453
$Zn_{0.75}Ni_{0.25}Fe_2O_4$	580	424
$Zn_{0.5}Ni_{0.5}Fe_2O_4$	590	423
$Zn_{0.25}Ni_{0.75}Fe_2O_4$	603	420
$NiFe_2O_4$	615	408

increase as a result of the lowering of the crystal symmetry. In the present work, for all the $Zn_{1-x}Ni_xFe_2O_4$ samples, no fine structure was detected in the IR spectra, whatever the annealing temperature was. Consequently, no order between the mixed transition ions could be evidenced at any temperature.

4. Conclusion

Single-phase well-crystallized nanosized ferrites $Zn_{1-x}Ni_xFe_2O_4$ ($x = 0$, 0.25, 0.5, 0.75, 1) were successfully obtained, from nitrate precursors, via a citrate–ethylene glycol method, at a relatively low temperature (650 °C). XRD studies combined with IR data show no evidence for a cation exchange or cation ordering in any of the specimen. Increasing the annealing temperature increases the grain size growth, observed from the SEM images which was correlated to the decreasing of the BET-surface areas, calculated from N_2-adsorption/desorption isotherms. For specimen subjected to similar heat treatments, Ni-rich solid solutions led to larger surface areas together with smaller particles.

Because the catalytic and magnetic properties of the $Zn_{1-x}Ni_xFe_2O_4$ compounds might depend on cation distribution, neutron powder diffraction studies are underway to reach the fractional occupancies of the transition metal at the tetrahedral and octahedral sites of the spinel structure. Differential scanning calorimetry analysis is in progress to check for temperature-dependent phase transitions associated to order–disorder phenomena and to reach the thermodynamics and kinetics parameters that control the crystal structure equilibrium. Raman and ^{57}Fe Mössbauer spectroscopy as well as extended X-ray-absorption fine-structure studies will be carried out to check for short-range order effects on the catalytic properties.

Acknowledgments

We thank J. Le Lannic, Y. Le Gal and Dr. O. Merdrignac for their help with the SEM, IR and BET measurements.

References

[1] C.P. Marshall, W.A. Dollase, Am. Miner. 69 (1984) 928.
[2] S.V. Manorama, L. Satyanarayana, K. Madhusudan-Reddy, Sensors Actuators B Chem. 89 (2003) 62.
[3] C.S. Kim, H.M. Ko, W.H. Lee, J. Appl. Phys. 73 (1993) 6298.
[4] C.S. Kim, W.C. Kim, S.Y. An, S.W. Lee, J. Magn. Magn. Mater. 215–216 (2000) 213.
[5] M.P. Pechini, US Patent 3,330,697 (July 11, 1967).
[6] J. Rodriguez-Carvajal, Powder diffraction, in: Satellite Meeting of the 15th Congress of IUCr, Toulouse, France, 1990, p. 127.
[7] J. Rodriguez-Carvajal, Physica B 192 (1992) 55.
[8] A.M. El Sayed, Ceram. Int. 28 (2002) 363.
[9] K. Tsukimura, S. Sasaki, N. Kimizuka, Jpn. J. Appl. Phys. 36 (1997) 3609.
[10] H.S.C. O'Neill, Eur. J. Min. 4 (1989–1992) 571.
[11] C.N. Chinnasamy, A. Narayanasamy, N. Ponpandian, K. Chattopadhyay, K. Shinoda, B. Jeyadevan, K. Tohji, K. Nakatsuka, T. Furubayashi, I. Nakatani, Phys. Rev. B. 63 (2001) 4108.
[12] J.C. Waerenborgh, M.O. Figueiredo, J.M.P. Cabral, L.C.J. Pereira, J. Solid State Chem. 111 (1994) 300.
[13] A. Pavese, D. Levy, A. Hoser, Am. Miner. 85 (2000) 1497.
[14] N.L. Pakhomova, V.N. Belogurov, V.A. Bylinkin, A.M. Vinnik, L.M. Kassimenko, P.E. Senkov, Sov. Phys. Solid State 19 (1977) 1060.
[15] R.K. Puri, U. Varshney, J. Phys. Chem. Solids 44 (1983) 655.
[16] H.S.C. O'Neill, A. Navrotsky, Am. Miner. 69 (1984) 733.
[17] E. Wolska, P. Piszora, K. Stempin, C.R.A. Catlow, J. Alloys Compd. 286 (1999) 203.
[18] S.M. Woodley, C.R.A. Catlow, P. Piszora, K. Stempin, E. Wolska, J. Solid State Chem. 153 (2000) 310.
[19] S.V. Kakatkar, S.S. Kakatkar, R.S. Patil, A.M. Sankpal, S.S. Suryavanshi, D.N. Bhosale, S.R. Sawant, Phys. Stat. Sol. (b) 198 (1996) 853.
[20] H.H. Joshi, R.G. Kulkarni, J. Mater. Sci. 21 (1986) 2138.
[21] E. Wolska, K. Stempin, O. Krasnowska-Hobbs, Solid State Ionics 101–103 (1997) 527.
[22] P. Strobel, A. Ibarra-Palos, A. Michel, C. Poinsignon, A. Crisci, Solid State Sci. 5 (2003) 1009.
[23] V.A.M. Brabers, Phys. Stat. Sol. 33 (1969) 563.
[24] S. Hafner, Z. Krist. 115 (1961) 331.
[25] R.D. Waldron, Phys. Rev. 99 (1955) 1727.